energies

MDPI

Article

A Multi-Component Additive to Improve the Thermal Stability of $Li(Ni_{1/3}Co_{1/3}Mn_{1/3})O_2$-Based Lithium Ion Batteries

Qingsong Wang [1,2,*], Lihua Feng [1] and Jinhua Sun [1]

[1] State Key Laboratory of Fire Science, University of Science and Technology of China, Hefei 230026, China; flnflh@126.com (L.F.); sunjh@ustc.edu.cn (J.S.)

[2] Chinese Academy of Sciences Key Laboratory of Materials for Energy Conversion, University of Science and Technology of China, Hefei 230026, China

* Correspondence: pinew@ustc.edu.cn; Tel.: +86-551-6360-6455; Fax: +86-551-6360-1669

Academic Editor: Peter J S Foot

Received: 31 March 2016; Accepted: 23 May 2016; Published: 30 May 2016

Abstract: To improve the safety of lithium ion batteries, a multi-component (MC) additive (consisting of vinylene carbonate (VC), 1,3-propylene sulfite (PS) and dimethylacetamide (DMAC)) is used in the baseline electrolyte (1.0 M $LiPF_6$/ethylene carbonate (EC) + diethyl carbonate (DEC)). The electrolyte with the MC additive is named safety electrolyte. The thermal stabilities of fully charged $Li(Ni_{1/3}Co_{1/3}Mn_{1/3})O_2$ (NCM) mixed with the baseline electrolyte and safety electrolyte, respectively, are investigated using a C80 micro-calorimeter. The electrochemical performances of the NCM/baseline electrolyte/Li and NCM/safety electrolyte/Li half cells are evaluated using galvanostatic charge/discharge, cyclic voltammetry and alternating current (AC) impedance. The experimental results demonstrate that the fully charged NCM-safety electrolyte system releases less heat and reduces the main sharp exothermic peak value to a great extent, with a reduction of 40.6%. Moreover, the electrochemical performances of NCM/safety electrolyte/Li half cells are not worse, and are almost as good as that of the NCM/baseline electrolyte/Li half cells.

Keywords: lithium ion battery (LIB) safety; multi-component (MC) additive; thermal stability; electrolyte

1. Introduction

Lithium ion batteries have experienced a rapid commercialization, and are considered to be the most promising energy storage medium, because of their long-term cycle performance, high operating voltage, and higher energy density. These superior characteristics expand their application to electric vehicles, and the global demand for lithium ion batteries is still increasing year by year [1–3]. Lithium ion batteries contains flammable organic electrolytes and under certain abuse conditions, flames or smoke may be caused [4–7]. Therefore, safety has always been an issue for lithium ion batteries, especially for the larger size ones [8–11]. In order to enhance the safety of lithium ion batteries, many flame retardant additives for electrolytes have been developed. Tris-(2,2,2-trifluoroethyl) phosphate (TFP), and dimethyl methylphosphonate (DMMP) have been found to be able to reduce the flammability of the electrolytes, while simultaneously improving the cycling performance of the cell [12–15]. The common electrolytes which are added into the flame retardant additives can result in non-flammability or at least retard flammability of the whole electrolyte system, which is an efficient solution for the thermal safety of the lithium ion battery (LIB). To keep the electrochemical performance, the amount of flame retardant additives in the electrolyte should not beyond 20% either by weight or by volume [16–19]. Choi *et al.* [20] reported that the BMP-PF_6 can be used as a flame retardant additive. The optimum BMP-PF_6 content in the electrolyte is 10 wt % for improving safety without degrading

cycle performance of the cell. However some additives still decrease the batteries' electrochemical performance more or less [19,21,22].

As a strong polar aprotic solvent, dimethylacetamide (DMAC) is widely used in synthetic materials, petroleum chemicals, reaction catalysts, electrolytic solvents, and the adhesive industry, as well as a variety of crystalline adducts and complexes due to its unique physical and chemical properties. The interest in DMAC is also due to its stability, presumably due to hydrogen bonds or dipole-dipole interactions between the external N–H bonds and the solvent [23]. In our previous work, we have reported the use of "safety electrolyte", a mixture of vinylene carbonate (VC), 1,3-propylene sulfite (PS) and DMAC, as a multi-component (MC) LIB electrolyte additive. Table 1 shows the thermodynamics of baseline and safety electrolytes. The results imply that after adding the MC additive to the baseline electrolyte, the burning rate is reduced, the total heat generation of the electrolyte is decreased from −298.2 J/g to −162.1 J/g (a 45.6% drop), the exothermic onset temperature is delayed to 217.2 °C, and the major exothermic peak is extended from 201.4 °C to 244.2 °C [24]. However, in the actual lithium-ion battery system, the electrolyte coexists with electrodes, and therefore, the thermal stability of the coexisting system is closely related to the safety of lithium ion batteries. In this work, the thermal stability of electrolyte (with and without MC additive) coexisting with $Li(Ni_{1/3}Co_{1/3}Mn_{1/3})O_2$ (NCM) were mainly investigated, and the electrochemical performance of the half cells were also examined.

Table 1. Thermodynamics of baseline and safety electrolytes.

Electrolyte	Exothermic onset Temperature (°C)	Exothermic Peak (°C)	Heat Generation (J/g)
Baseline Electrolyte	181.8	201.4	−298.2
Safety Electrolyte	217.2	244.2	−162.1

2. Experimental

All the chemicals used in this work were commercially available and used as received. An electrolyte with 1.0 mol/L $LiPF_6$ in a mixture of 1:1 (wt %) ethylene carbonate (EC) and diethyl carbonate (DEC) was selected as a baseline electrolyte. The safety electrolyte was the mixture of MC additive and the mentioned electrolyte (1.0 M $LiPF_6$/EC + DEC) at the certain weight ratio (wt %), which was manipulated in an argon glove box. NCM was used to prepare a cathode electrode laminate.

Cathode electrodes consisting of NCM (90 wt %), acetylene black (5 wt %), and polyvinylidene fluoride (PVDF) (5 wt %) and a Celgard 2400 polyethylene separator (25 μm thick) were used. The cathode electrode was dried overnight in vacuum at 80 °C, then handled in the argon filled glove box (SG2400/750TS, Vigor, Suzhou, China, <1 ppm O_2 and H_2O). The electrodes were punched in disk-shaped pieces of 14 mm diameter and 200 μm thickness.

For the battery thermal test, the NCM/baseline electrolyte/Li and NCM/safety electrolyte/Li half cells were cycled three times between 2.0 V and 4.2 V at 0.1C, then charged to 4.2 V and held for 1 h to ensure their voltage remained at 4.2 V before they were disassembled. After the upper cutoff voltage was obtained, the charged cells were disassembled in a glove box and the cathode electrode was taken out. To purge the electrode of the original electrolyte, the wet charged electrode powder was placed into a bottle. To this bottle, DEC was added and the bottle was then shaken by hand. The sample was then decanted and the DEC rinsing procedure was repeated. After drying the electrode to remove DEC, the charged cathode electrode materials were scraped from the Al foil carefully and were prepared for later thermal tests.

In the C80 micro-calorimeter measurements, the electrolyte solutions were prepared in the glove box, then the electrolytes and prepared cathode electrode materials were transferred from the argon-filled glove box into an 8.5 mL in volume high pressure stainless steel vessel, mixed, and then the vessel was sealed in an argon atmosphere. For the same kind of cathode electrode material, the mass of mixed electrolyte and electrode in each sample was approximately equal, and the mass ratio

between cathode electrode and electrolyte was 1.8:1. In order to verify that the system was hermetically sealed, before and after the experiment, the weight of each sample (vessel + sample) was measured. The weight was constant in all cases, indicating that there were no leaks during the experiments. The heating rate was set at 0.2 °C/min from ambient temperature to 300 °C and the C80 calculations were based on the sample mass.

The effect of the three additives on the cell performance was tested in CR2032 coin cells of NCM/Li. The cell performance was determined on a multi-channel battery cycler (Neware BTS-6V 10 mA, Shenzhen, China) by assembling CR2032 coin cells of NCM/Li in the glove box. These cells were cycled between a set range of voltages (NCM/Li: 2.0–4.2 V) at 0.1C. The electrochemical stability of the electrolytes on the electrodes was measured by cyclic voltammetry (CV) using the above coin cells at a scan rate of 0.1 mV/s on a 604A Electrochemical Workstation (CHI, Shanghai, China). The alternating current (AC) impedance was also measured with the CHI 604A Electrochemical Workstation, with the frequency range and voltage amplitude set as 100 kHz to 0.01 Hz and 5 mV, respectively.

3. Results and Discussion

3.1. Thermal Stability

Figure 1 shows the heat flow curves of charged NCM-baseline electrolyte and NCM-safety electrolyte systems at the 0.2 °C/min heating rate. The charged NCM was obtained from NCM/electrolyte/Li half cells at 4.2 V with safety electrolyte and baseline electrolyte.

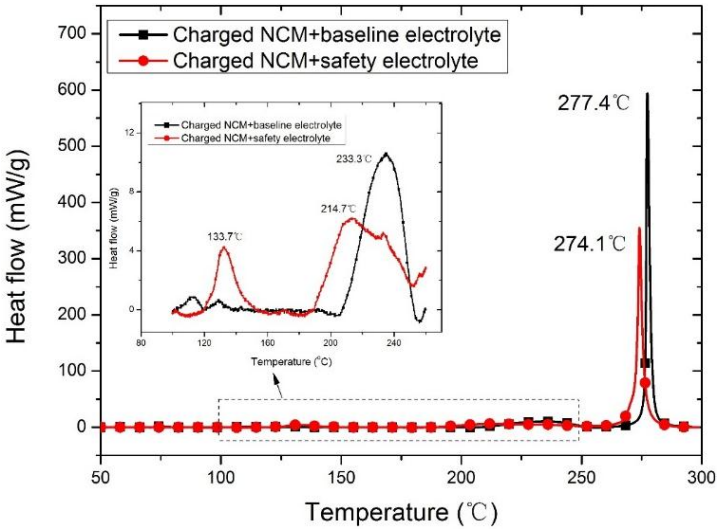

Figure 1. C80 heat flow of NCM-baseline electrolyte and NCM-safety electrolyte system in argon filled vessel at a 0.2 °C/min heating rate. The NCM were extracted from NCM/safety electrolyte/Li and NCM/baseline electrolyte/Li half cells at 4.2 V.

In the NCM-baseline electrolyte system, the total heat generation is −486.6 J/g. A mild exothermic process was detected at 233.3 °C with the heat generation of −83.3 J/g, and then an extremely sharp exothermic peak occurs at 277.4 °C with the heat output of −403.3 J/g. In terms of the NCM-safety electrolyte system, the total heat generation is reduced to −467.0 J/g. At the earlier 133.7 °C, one mild exothermic process was detected, and the other mild exothermic process occurs at 214.7 °C with the heat generation of −76.4 J/g. Similarly, in the NCM-safety electrolyte system, a sharp exothermic peak is seen at 274.1 °C with a heat output of −373.5 J/g. Though the sharp exothermic peak of NCM-safety electrolyte system is a bit earlier (274.1 °C < 277.4 °C), for the normal LIB, thermal runaway has already occurred before 274 °C. Therefore, the slightly earlier onset of the exothermic peak has no effect on the LIB safety. In addition, the NCM-safety electrolyte system releases less heat, and the

sharp peak value reduces from 594.2 mW/g to 352.7 mW/g, with a reduction of 40.6%, which will make a great contribution to the safety of thermal runaway batteries. The heat flow curves of baseline and safety electrolytes have a broad exothermic process at 233.3 °C and 214.7 °C, respectively, which are correlated to the decomposition of NCM [25]. The extremely sharp exothermic peaks, located at around 275 °C, are attributable to high reactivity between the delithiated NCM cathode electrode and electrolyte [26,27]. The highly delithiated NCM reacts with the organic electrolyte, which releases oxygen and causes a thermal runaway [25,28].

Figure 2 shows the heat flow curves of VC, PS, and DMAC at a 0.2 °C/min heating rate. VC, PS, and DMAC give rise to onset temperatures of around 85.3 °C, and then reach their endothermic peak temperatures at 182.5, 186.4 and 199.3 °C, with total heat absorptions of 326.7, 226.5, and 321.8 J/g, respectively. All of them only have an endothermic process, and no exothermic processes were detected. For this reason, the NCM-safety electrolyte system releases less heat, and the main sharp peak value apparently decreases much more than that of the NCM-baseline electrolyte system.

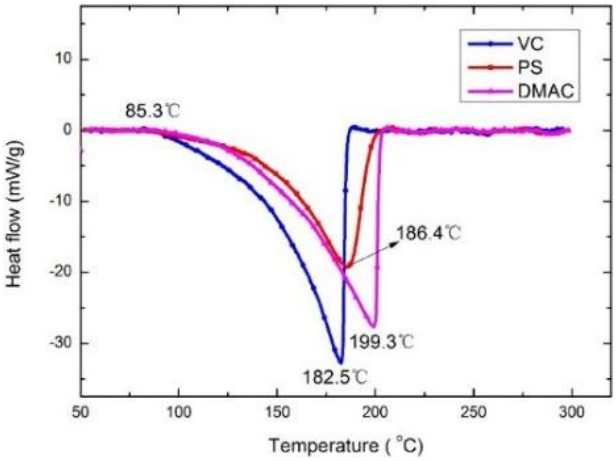

Figure 2. C80 Heat flow profiles of vinylene carbonate (VC), propylene sulfite (PS), and dimethylacetamide (DMAC) at a 0.2 °C/min heating rate.

In summary, the above thermal investigations results are adequate to evaluate the thermal stability of the electrode/electrolyte system, and they suggest that the MC additive in the electrolyte generates less heat, and significantly reduces the main sharp peak value, which can improve the thermal stability of the NCM LIB.

3.2. Electrochemical Performance

Figure 3 is the cycle efficiency of NCM/baseline electrolyte/Li and NCM/safety electrolyte/Li half cells between 2.0 V and 4.2 V at 0.1C cycling rate. The mean cycle efficiencies of NCM/baseline electrolyte/Li and NCM/safety electrolyte/Li half cells are 98.27% and 98.70%, with standard deviations of 1.82 and 1.31, respectively. Here the standard deviation is clustered around the mean in a set of data. If the data are quite tightly bunched together, the standard deviation is small, but if they are widely spread, the standard large deviation is large [29]. These data show that the mean cycle efficiency of NCM/safety electrolyte/Li half cells is higher and the standard deviation is smaller, suggesting that the addition of MC additive does not worsen the cycle efficiency.

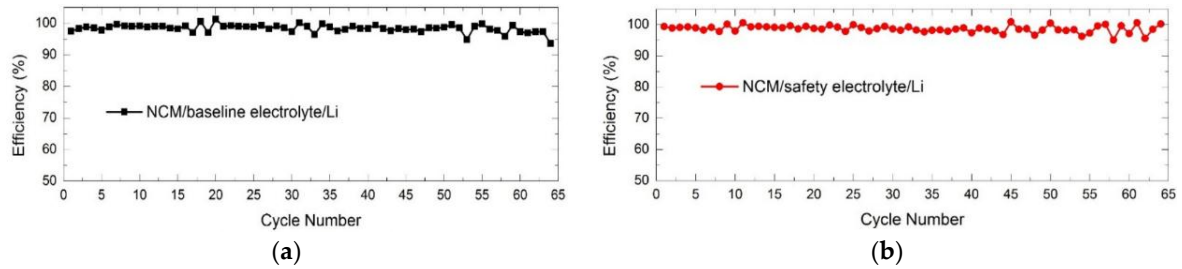

Figure 3. Cycle efficiency of half cells. The half cells were cycled between 2.0 V and 4.2 V at 0.1C: (**a**) NCM/baseline electrolyte/Li half cells; (**b**) NCM/safety electrolyte/Li half cells.

Figure 4 illustrates the cycling performance of the NCM/Li half cells with baseline and safety electrolytes charged and discharged at 0.1C within the potential range of 2.0–4.2 V. Discharge capacity was calculated based on the mass of NCM. It can be seen that from the first cycle to the 65th cycle, the two half cells' specific capacity decreases gradually. For the NCM/safety electrolyte/Li half cells, the specific capacity changes from 147 mAh/g to 137 mAh/g, and the capacity retention reaches values as high as 93.2%. Some safety additives sacrifice the partial specific capacity in order to obtain effective safety results [19,30–32]. However, with the addition of the MC additive, the cycling performance of NCM/safety electrolyte/Li half cells does not become worse. It can be speculated that the higher electrolyte conductivity makes a favorable contribution [24].

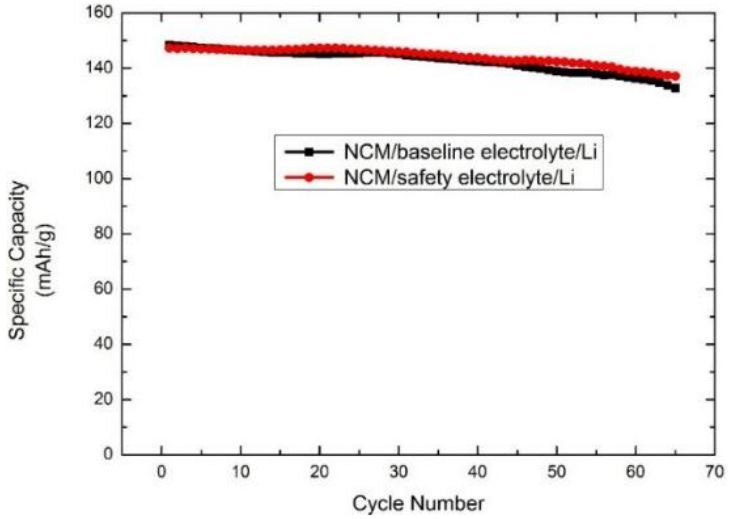

Figure 4. Cycle performance at 0.1C of NCM/baseline electrolyte electrolyte/Li and NCM/safety/Li half cells. The half cells were cycled between 2.0 V and 4.2 V at 0.1C.

To further inspect the relationship between the specific capacity and voltage in the various cycles, the charge/discharge capacity curves of the two half cells for different cycles are shown in Figure 5. At the first cycle, the flat charge of the NCM/safety electrolyte/Li half cells is a bit higher, and the discharge specific capacity curves coincide completely. With the increasing number of the cycles, at the 65th cycle (Figure 5b), the charge specific capacity curve is exactly the same, but compared to that of the NCM/safety electrolyte/Li half cells, the discharge specific capacity of the NCM/baseline electrolyte/Li half cells becomes smaller.

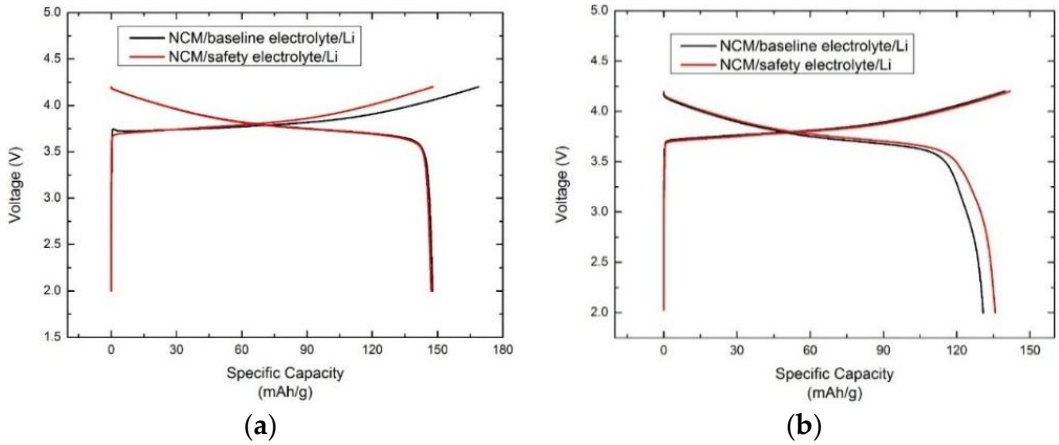

Figure 5. Charge/discharge plots of NCM/baseline electrolyte electrolyte/Li and NCM/safety electrolyte/Li half cells. The half cells were cycled between 2.0 V and 4.2 V at 0.1C: (**a**) 1st cycle; and (**b**) 65th cycle.

Figure 6 shows the CV curves of NCM/baseline electrolyte/Li and NCM/safety electrolyte/Li half cells. The CV tests were carried out with a potential sweep rate of 0.1 mV/s over the potential range from 2.0 V to 4.2 V at room temperature. Each curve has a pair of oxidation-reduction peaks, respectively, which correspond to the intercalation and extraction of Li-ion. It can be seen that the sharp oxidation peaks locate at around 3.9 V (*i.e.*, lithiation) followed by a broader reduction feature during delithiation at around 3.6 V. The peaks can be related to the redox couple of $Ni^{2+/4+}$, while Mn^{4+} are known to be electrochemically inactive. The $Co^{3+/4+}$ disappears since their redox reaction takes place at a potential range of 4.55–4.65 V, which is bigger than 4.2 V. The minor amounts of Ni^{3+} were not clearly shown in CV [33]. Hence, within the 2.0–4.2 V potential range, only the couple of $Ni^{2+/4+}$ redox peaks were detected. The oxidation and reduction process can be shown by reactions below [34]:

$$\mathrm{Li}\left(\mathrm{Ni}_{1/3}\mathrm{Co}_{1/3}\mathrm{Mn}_{1/3}\right)\mathrm{O}_2 \rightleftarrows \mathrm{Li}_{1-x}\left(\mathrm{Ni}_{1/3}\mathrm{Co}_{1/3}\mathrm{Mn}_{1/3}\right)\mathrm{O}_2 + x\mathrm{Li}^+ + x\mathrm{e}^-$$

where the x value depends on the charge/discharge state of NCM at different potential ranges. It can be seen that in the NCM/baseline electrolyte/Li system, two reduction peaks were detected at 3.5 V and 3.7 V, respectively, at the first cycle. Nevertheless, in the NCM/safety electrolyte/Li system, only a broader reduction peak can be found at 3.7 V at the first cycle.

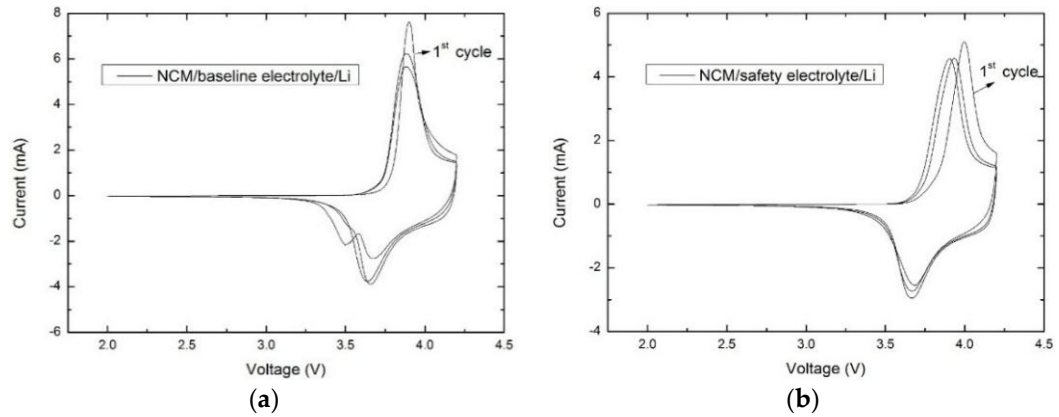

Figure 6. Cyclic voltammograms (CV) of NCM/Li half cells with different electrolytes: (**a**) NCM/baseline electrolyte/Li; and (**b**) NCM/safety electrolyte/Li.

The reason of the appearance of the misshapen reduction peak at the first cycle after the addition of the MC additive is not clear, but in the sequent cycles, the CV curves of NCM/safety electrolyte/Li system almost show the same trace, indicating that the safety electrolyte has a good stability and compatibility on the NCM electrode. It is worth mentioning that there are no obvious double plateaus (Figure 6a) corresponding to the two reduction peaks, perhaps because the galvanostatical charge at the constant current can overcome some kinetic effect more easily than the non-constant current during the cyclic voltammetry test [31].

The AC impedance spectra of the NCM/baseline electrolyte/Li and NCM/safety electrolyte/Li half cells which were cycled three times between 2.0 V and 4.2 V at 0.1C, and discharged to the voltage of 3.75 V, respectively, are shown in Figure 7. The simulation results were obtained by Z-view software and using the same equivalent circuit. It can be found that the experimental and simulated AC impedance curves are almost coincident, which indicates that the AC impedance spectrum agree well with the equivalent circuit. An equivalent circuit can represent the electrode/electrolyte system (Figure 8). Instead of using the capacitance of solid electrolyte interphase (SEI) film and double-layer capacitance of electrodes, the constant phase elements (CPE1) of the SEI film and the constant phase elements (CPE2) of the electrode were used. According to the equivalent circuit, the intersection of the AC impedance diagram with the real axis refers to the bulk resistance (R_b), which shows electric resistance of the electrolyte, separator, and electrodes. Each plot has a superposition of two semicircles, one is in the high frequency region and is attributed to resistance of the surface film (R_{sei}) covering on the NCM cathode electrode, the other in the mid-frequency region approximately represents charge transfer resistance (R_{ct}). The slope line at low frequency corresponds to the diffusion of the lithium ions into the bulk of the electrode material or so-called Warburg diffusion [35–38].

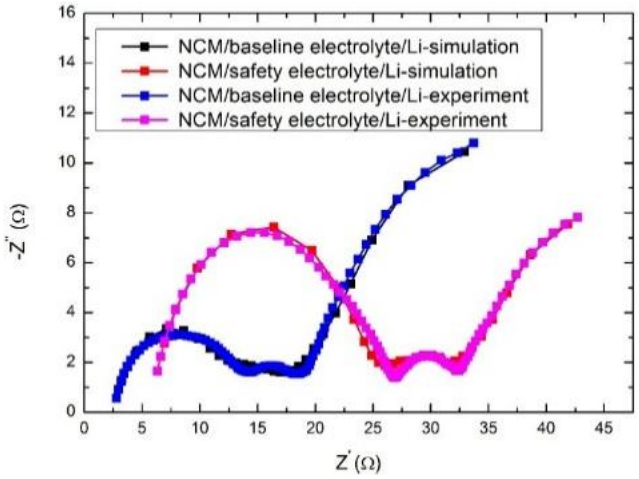

Figure 7. AC impedances of NCM/baseline electrolyte/Li and NCM/safety electrolyte/Li half cells. The half cells were cycled there times between 2.0 V and 4.2 V and then were discharged approximately to 3.75 V.

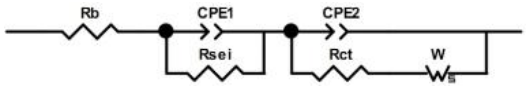

Figure 8. An equivalent circuit representing the electrode/electrolyte system.

Table 2 shows the parameters of the recorded equivalent circuit. According to the simulation results, the R_b value of NCM/safety electrolyte/Li half cell is 5.651 Ω, which is bigger than that of NCM/baseline electrolyte/Li half cell (R_b = 2.487 Ω). It can be found that both the R_{sei} values are bigger as compared to the R_{ct} value during the three cycles, revealing that the electrochemical

performance is mainly influenced by the surface film resistance. It can be seen that the R_{sei} value of NCM/safety electrolyte/Li half cell (R_{sei} = 17.56 Ω) is much bigger than that of NCM/baseline electrolyte/Li half cell (R_{sei} = 8.172 Ω), suggesting that more side reaction takes place between NCM electrode and the safety electrolyte, leading to the formation of SEI layer with higher resistance.

Table 2. Resistance parameters of R_b, R_{sei} and R_{ct} obtained from simulation data.

Half Cell	R_b (Ω)	R_{sei} (Ω)	R_{ct} (Ω)
NCM/baseline electrolyte/Li	2.487	8.172	7.608
NCM/safety electrolyte/Li	5.651	17.56	10.380

The surface morphology of the NCM electrodes taken from the half cells after 65 cycles were observed by scanning electron microscope (SEM), the obtained results are presented in Figure 9. After cycling, Figure 9b,c shows deposits on the NCM surface formed from the electrolyte decomposition. The deposits can be regarded as the SEI films because lithium ions can transport through them during the charge/discharge cycle [39], in addition, the deposit images look different. The deposit appears on the NCM electrode cycled in the safety electrolyte pads more gaps than that of the Figure 9b, suggesting that there is more deposit formed on the NCM electrode in the safety electrolyte, which is coincident with the results of AC impedance, hence in the thermal stability test, its heat of breakdown was apparent at 133.7 °C, and the heat of breakdown of deposit on NCM electrode cycled in the baseline electrolyte is mild, as shown in Figure 1.

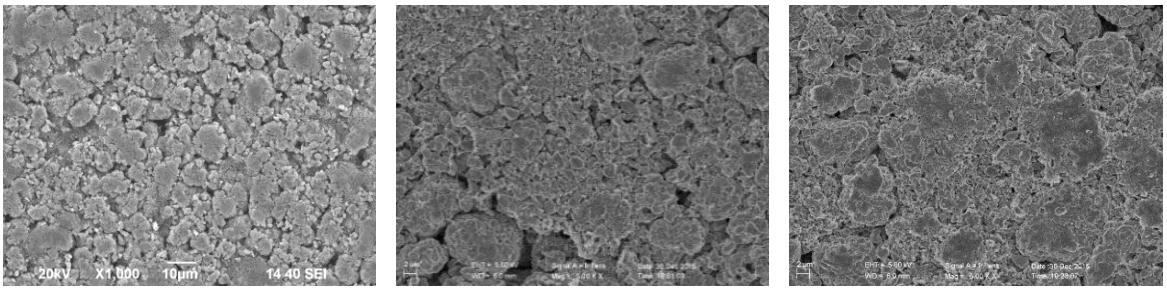

(**a**) (**b**) (**c**)

Figure 9. Scanning electron microscope (SEM) analysis before and after three cycles: (**a**) fresh NCM cathode electrode; (**b**) NCM cathode electrode cycled in baseline electrolyte; and (**c**) NCM cathode electrode cycled in safety electrolyte.

4. Conclusions

The safety electrolyte that has been validated in our previous work shows good safety, thermal stability and conductivity. The effects of the safety electrolyte on NCM electrode were investigated in this work. It was found that the MC additive (*i.e.*, VC, PS, and DMAC) only had an endothermic process in the thermal stability test, leading to the less heat generation of a fully charged NCM-safety electrolyte system, and a drastic reduction of the main exothermic peak value, which improved the thermal stability of the NCM LIB. In the electrochemical performance tests, NCM/safety electrolyte/Li half cells exhibited more stable cycle efficiency and good specific capacity retention, and CV results indicated that the safety electrolyte had good stability and compatibility with NCM. The results of AC impedance and SEM images show that the R_{sei} value of NCM/safety electrolyte/Li half cells was bigger, and deposits appear on the NCM electrode cycled in the safety electrolyte padded with more gaps, which explained the mild exothermic process at 133.7 °C of NCM/safety electrolyte/Li heat flow curves. To popularize the application of MC additive in LIB, studies on how MC additive would behave on the anodes and full cell, will be carried out.

Acknowledgments: This work is supported by the National Natural Science Foundation of China (No. 51176183), the External Cooperation Program of Bureau of International Co-operation, Chinese Academy of Sciences (No. 211134KYSB20150004), and the Fundamental Research Funds for the Central Universities (No. WK2320000034). Qingsong Wang is supported by Youth Innovation Promotion Association Chinese Academy of Sciences (No. 2013286).

Author Contributions: Lihua Feng performed the experiments, analyzed the data and wrote the paper; Qingsong Wang supervised the whole process of this work; Jinhua Sun improved the paper.

Conflicts of Interest: The authors declare no conflict of interest.

References

1. Hsieh, C.T.; Chen, Y.F.; Pai, C.T.; Mo, C.Y. Synthesis of lithium nickel cobalt manganese oxide cathode materials by infrared induction heating. *J. Power Sources* **2014**, *269*, 31–36. [CrossRef]
2. Sa, Q.; Gratz, E.; He, M.; Lu, W.; Apelian, D.; Wang, Y. Synthesis of high performance $LiNi_{1/3}Mn_{1/3}Co_{1/3}O_2$ from lithium ion battery recovery stream. *J. Power Sources* **2015**, *282*, 140–145. [CrossRef]
3. Kang, K.S.; Choi, S.; Song, J.; Woo, S.G.; Jo, Y.N.; Choi, J.; Yim, T.; Yu, J.S.; Kim, Y.J. Effect of additives on electrochemical performance of lithium nickel cobalt manganese oxide at high temperature. *J. Power Sources* **2014**, *253*, 48–54. [CrossRef]
4. Wrodnigg, G.H.; Besenhard, J.O.; Winter, M. Cyclic and acyclic sulfites: new solvents and electrolyte additives for lithium ion batteries with graphitic anodes? *J. Power Sources* **2001**, *97*, 592–594. [CrossRef]
5. Isken, P.; Dippel, C.; Schmitz, R.; Schmitz, R.; Kunze, M.; Passerini, S.; Winter, M.; Lex-Balducci, A. High flash point electrolyte for use in lithium-ion batteries. *Electrochim. Acta* **2011**, *56*, 7530–7535. [CrossRef]
6. Wrodnigg, G.H.; Wrodnigg, T.M.; Besenhard, J.O.; Winter, M. Propylene sulfite as film-forming electrolyte additive in lithium ion batteries. *Electrochem. Commun.* **1999**, *1*, 148–150. [CrossRef]
7. Schmitz, R.; Schmitz, R.; Müller, R.; Kazakova, O.; Kalinovich, N.; Röschenthaler, G.V.; Winter, M.; Passerini, S.; Lex-Balducci, A. Methyl tetrafluoro-2-(methoxy) propionate as co-solvent for propylene carbonate-based electrolytes for lithium-ion batteries. *J. Power Sources* **2012**, *205*, 408–413. [CrossRef]
8. Wang, Q.; Sun, J.; Yao, X.; Chen, C. C80 calorimeter studies of the thermal behavior of $LiPF_6$ solutions. *J. Solut. Chem.* **2006**, *35*, 179–189. [CrossRef]
9. Doughty, D.H.; Roth, E.P.; Crafts, C.C.; Nagasubramanian, G.; Henriksen, G.; Amine, K. Effects of additives on thermal stability of Li ion cells. *J. Power Sources* **2005**, *146*, 116–120. [CrossRef]
10. Ritchie, A. Recent developments and likely advances in lithium rechargeable batteries. *J. Power Sources* **2004**, *136*, 285–289. [CrossRef]
11. Wang, Q.; Sun, J.; Yao, X.; Chen, C. Micro calorimeter study on the thermal stability of lithium-ion battery electrolytes. *J. Loss Prev. Process Ind.* **2006**, *19*, 561–569. [CrossRef]
12. Zhang, S.S. A review on electrolyte additives for lithium-ion batteries. *J. Power Sources* **2006**, *162*, 1379–1394. [CrossRef]
13. Xu, K.; Zhang, S.; Allen, J.L.; Jow, T.R. Evaluation of fluorinated alkyl phosphates as flame retardants in electrolytes for Li-ion batteries: II. Performance in cell. *J. Electrochem. Soc.* **2003**, *150*, A170–A175. [CrossRef]
14. Xiang, H.; Jin, Q.; Chen, C.; Ge, X.; Guo, S.; Sun, J. Dimethyl methylphosphonate-based nonflammable electrolyte and high safety lithium-ion batteries. *J. Power Sources* **2007**, *174*, 335–341. [CrossRef]
15. Xiang, H.; Xu, H.; Wang, Z.; Chen, C. Dimethyl methylphosphonate (DMMP) as an efficient flame retardant additive for the lithium-ion battery electrolytes. *J. Power Sources* **2007**, *173*, 562–564. [CrossRef]
16. Hyung, Y.E.; Vissers, D.R.; Amine, K. Flame-retardant additives for lithium-ion batteries. *J. Power Sources* **2003**, *119*, 383–387. [CrossRef]
17. Yao, X.; Xie, S.; Chen, C.; Wang, Q.; Sun, J.; Li, Y.; Lu, S. Comparative study of trimethyl phosphite and trimethyl phosphate as electrolyte additives in lithium ion batteries. *J. Power Sources* **2005**, *144*, 170–175. [CrossRef]
18. Mandal, B.K.; Padhi, A.K.; Shi, Z.; Chakraborty, S.; Filler, R. Thermal runaway inhibitors for lithium battery electrolytes. *J. Power Sources* **2006**, *161*, 1341–1345. [CrossRef]
19. Wang, Q.; Sun, J.; Yao, X.; Chen, C. 4-Isopropyl phenyl diphenyl phosphate as flame-retardant additive for lithium-ion battery electrolyte. *Electrochem. Solid-State Lett.* **2005**, *8*, A467–A470. [CrossRef]

20. Choi, J.A.; Sun, Y.K.; Shim, E.G.; Scrosati, B.; Kim, D.W. Effect of 1-butyl-1-methylpyrrolidinium hexafluorophosphate as a flame-retarding additive on the cycling performance and thermal properties of lithium-ion batteries. *Electrochim. Acta* **2011**, *56*, 10179–10184. [CrossRef]
21. Wang, Q.; Ping, P.; Sun, J.; Chen, C. Cresyl diphenyl phosphate effect on the thermal stabilities and electrochemical performances of electrodes in lithium ion battery. *J. Power Sources* **2011**, *196*, 5960–5965. [CrossRef]
22. Wang, Q.; Sun, J.; Chen, C. Enhancing the thermal stability of $LiCoO_2$ electrode by 4-isopropyl phenyl diphenyl phosphate in lithium ion batteries. *J. Power Sources* **2006**, *162*, 1363–1366. [CrossRef]
23. Liu, F.; Tian, W.; Yang, X.; Jia, G. Hydrogen-bonding and dielectric response of N,N-dimethylacetamide aqueous solutions under E/M fields using molecular dynamics. *J. Mol. Liq.* **2014**, *197*, 100–105. [CrossRef]
24. Feng, L.H.; Wang, Q.S.; Ai, C.Y.; Sun, J.H. The Effect of Multi-component Electrolyte Additive on $LiFePO_4$ Based Lithium Ion Batteries. In Proceedings of the 10th Asia-Oceania Symposium on Fire Science and Technology, Tsukuba, Japan, 5–7 October 2015.
25. Cho, J.; Jung, H.; Park, Y.; Kim, G.; Lim, H.S. Electrochemical properties and thermal stability of $Li_aNi_{1-x}CO_xO_2$ cathode materials. *J. Electrochem. Soc.* **2000**, *147*, 15–20. [CrossRef]
26. Hsieh, C.T.; Mo, C.Y.; Chen, Y.F.; Chung, Y.J. Chemical-wet synthesis and electrochemistry of $LiNi_{1/3}Co_{1/3}Mn_{1/3}O_2$ cathode materials for Li-ion batteries. *Electrochim. Acta* **2013**, *106*, 525–533. [CrossRef]
27. Wu, F.; Wang, M.; Su, Y.; Chen, S.; Xu, B. Effect of TiO_2-coating on the electrochemical performances of $LiCo_{1/3}Ni_{1/3}Mn_{1/3}O_2$. *J. Power Sources* **2009**, *191*, 628–632. [CrossRef]
28. Liu, S.; Xiong, L.; He, C. Long cycle life lithium ion battery with lithium nickel cobalt manganese oxide (NCM) cathode. *J. Power Sources* **2014**, *261*, 285–291. [CrossRef]
29. Wang, Q.; Ping, P.; Sun, J.; Chen, C. Improved thermal stability of lithium ion battery by using cresyl diphenyl phosphate as an electrolyte additive. *J. Power Sources* **2010**, *195*, 7457–7461. [CrossRef]
30. Zeng, Z.; Jiang, X.; Wu, B.; Xiao, L.; Ai, X.; Yang, H.; Cao, Y. Bis (2,2,2-trifluoroethyl) methylphosphonate: an novel flame-retardant additive for safe lithium-ion battery. *Electrochim. Acta* **2014**, *129*, 300–304. [CrossRef]
31. Xiang, H.F.; Jin, Q.Y.; Wang, R.; Chen, C.H.; Ge, X.W. Nonflammable electrolyte for 3-V lithium-ion battery with spinel materials $LiNi_{0.5}Mn_{1.5}O_4$ and $Li_4Ti_5O_{12}$. *J. Power Sources* **2008**, *179*, 351–356. [CrossRef]
32. Xu, K.; Zhang, S.; Allen, J.L.; Jow, T.R. Nonflammable electrolytes for Li-ion batteries based on a fluorinated phosphate. *J. Electrochem. Soc.* **2002**, *149*, A1079–A1082. [CrossRef]
33. Shaju, K.; Rao, G.S.; Chowdari, B. Performance of layered $Li(Ni_{1/3}Co_{1/3}Mn_{1/3})O_2$ as cathode for Li-ion batteries. *Electrochim. Acta* **2002**, *48*, 145–151. [CrossRef]
34. Yabuuchi, N.; Makimura, Y.; Ohzuku, T. Solid-state chemistry and electrochemistry of $LiCo_{1/3}Ni_{1/3}Mn_{1/3}O_2$ for advanced lithium-ion batteries II. Preparation and characterization. *J. Electrochem. Soc.* **2007**, *154*, A1434–A1440. [CrossRef]
35. Zheng, J.M.; Wu, X.B.; Yang, Y. A comparison of preparation method on the electrochemical performance of cathode material $Li[Li_{0.2}Mn_{0.54}Ni_{0.13}Co_{0.13}]O_2$ for lithium ion battery. *Electrochim. Acta* **2011**, *56*, 3071–3078. [CrossRef]
36. Oljaca, M.; Blizanac, B.; Du Pasquier, A.; Sun, Y.; Bontchev, R.; Suszko, A.; Wall, R.; Koehlert, K. Novel $Li(Ni_{1/3}Co_{1/3}Mn_{1/3})O_2$ cathode morphologies for high power Li-ion batteries. *J. Power Sources* **2014**, *248*, 729–738. [CrossRef]
37. Tan, L.; Liu, H. High rate charge–discharge properties of $LiNi_{1/3}Co_{1/3}Mn_{1/3}O_2$ synthesized via a low temperature solid-state method. *Solid State Ion.* **2010**, *181*, 1530–1533. [CrossRef]
38. He, Y.B.; Liu, M.; Huang, Z.D.; Zhang, B.; Yu, Y.; Li, B.; Kang, F.; Kim, J.K. Effect of solid electrolyte interface (SEI) film on cyclic performance of $Li_4Ti_5O_{12}$ anodes for Li ion batteries. *J. Power Sources* **2013**, *239*, 269–276. [CrossRef]
39. Li, B.; Wang, Y.; Rong, H.; Wang, Y.; Liu, J.; Xing, L.; Xu, M.; Li, W. A novel electrolyte with the ability to form a solid electrolyte interface on the anode and cathode of a $LiMn_2O_4$/graphite battery. *J. Mater. Chem. A* **2013**, *1*, 12954–12961. [CrossRef]